

Loss Minimization of Speed Controlled Induction Machines in Transient States Considering System Constraints

Zheng Hu^{*}, Qiang Liu^{*}, and Kay Hameyer^{*}, Senior Member, IEEE

Abstract – This paper proposes a new control scheme based on maximum torque-per-ampere (MTPA) for speed controlled induction machines. In the MTPA scheme the torque and flux-generating currents are calculated from the reference torque. In order to attain the reference torque in the constrained regions, the loss minimization curve can not be guaranteed anymore. Instead of the optimum current, the boundary values are chosen. In the new approach the reference torque in transient states will be adapted dynamically in such a way, that the loss minimization is always pursued. To track this loss minimization trajectory exactly, especially in transient states, an optimum current control scheme with generalized predictive control is introduced. The simulation results show that the energy losses can be reduced significantly when compared to the steady state MTPA during the transient procedure in constrained regions without deterioration of drive dynamic.

Keywords: Loss minimization, Induction motor

1. Introduction

Induction motors (IM) are applied in high performance electric drive systems because of their simple structure, low manufacturing cost and high reliability. However, due to the additional magnetization current the efficiency of IM is lower when compared to permanent-magnet synchronous machines[1]. proposes to improve the power efficiency by control means. Until now, there exist various control schemes to cope with this disadvantage. Maximum torque-per-ampere (MTPA) control realizes the loss minimization in steady states[2]. gives the control scheme in the complete operating region.

In principle the efficiency improvement control can be divided into three classes [3]: loss-model-based methods [4-8], self-optimizing methods [9-11] and hybrid methods. In model-based loss-minimization algorithms diverse loss models were developed. In [5] the loss model was simplified by neglecting the leakage inductance of stator and rotor, which causes inaccuracy of voltage description especially in high speed region. In [7] the loss model including leakage inductance was taken into account. However, the iron loss current was neglected for the simplification. The iron losses result from the air gap voltage. In high speed region, where the iron loss current is not neglectable, the modeled losses are inaccurate[8]. investigated the effect of stator resistance on the voltage constraint, which was not considered in previous works. The voltage ellipse rotates counterclockwise if the voltage

drop on stator resistance is incorporated into the voltage description. However, the computational effort is increased enormously. Because of its marginal impact this voltage term will not be considered in this study.

In this paper the iron loss current will be derived for iron loss calculation, so that the loss model is close to the full loss model over the whole speed region. The proposed scheme in this paper adjusts the required torque, flux- and torque-generating currents of speed controlled IM during the transient procedure in such a way, that the loss minimization is always pursued, especially in regions, where stator current and voltage are constrained.

The paper is organized as follows: in section II the machine dynamic model including losses is introduced, in which the iron loss current is considered. Based on this model the power loss formulation is derived. This power loss formulation is used for the proposed optimum current control with dynamic torque adaptation, which is discussed in section III. In section IV, the simulation results of the conventional $1/\omega_t$ [12], steady state MTPA and the proposed control schemes are presented.

2. Loss Modeling and Calculation

In consideration of iron loss for the fundamental wave model the entire losses can be calculated by stator and rotor copper losses as well as iron losses, whereat the coefficients of the latter two losses depend on the electrical angular frequencies of stator and rotor. In [7] the iron losses are approximated by the square of the air gap voltage divided by a constant, which can be considered as a resistance

^{*} Institute of Electrical Machines (IEM), RWTH Aachen University, Germany. (zheng.hu@iem.rwth-aachen.de)

connected in parallel to the mutual inductance. Due to the slip, the rotor iron losses are much smaller than the stator iron losses. Thus, rotor iron losses are neglected in this paper for purpose of computational simplification.

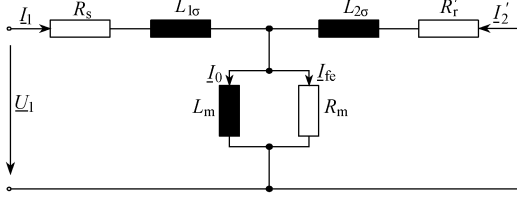


Fig. 1. Equivalent circuit diagram for induction motor including losses

In Fig. 1 the fundamental wave model of an IM with iron losses is given, where $I_{\underline{0}}$ and $I_{\underline{fe}}$ describes the currents flowing through mutual inductance and iron loss resistance, $L_{1\sigma}$ and $L'_{2\sigma}$ the leakage inductances of stator and rotor (referred to stator side), respectively. Therefore, the stator and rotor as well as air gap voltage equations in the synchronous frame can be given as follows:

$$u_{ds}^e = R_s i_{ds}^e + \frac{d}{dt} \Psi_{ds}^e - \omega_e \Psi_{qs}^e \quad (1)$$

$$u_{qs}^e = R_s i_{qs}^e + \frac{d}{dt} \Psi_{qs}^e + \omega_e \Psi_{ds}^e \quad (2)$$

$$0 = R_r' i_{dr}^e + \frac{d}{dt} \Psi_{dr}^e - (\omega_e - \omega_r) \Psi_{qr}^e \quad (3)$$

$$0 = R_r' i_{qr}^e + \frac{d}{dt} \Psi_{qr}^e + (\omega_e - \omega_r) \Psi_{dr}^e \quad (4)$$

$$R_m i_{dfe}^e = -\omega_e \Psi_{qm}^e \quad (5)$$

$$R_m i_{qfe}^e = \omega_e \Psi_{dm}^e \quad (6)$$

Where R_s , R_r' and R_m denote the stator, rotor (referred to stator side) and iron loss resistance; ω_e , ω_r the synchronous and rotor speed; u_{ds}^e , u_{qs}^e , i_{ds}^e , i_{qs}^e , i_{dr}^e , i_{qr}^e , i_{dfe}^e , i_{qfe}^e , Ψ_{ds}^e , Ψ_{qs}^e , Ψ_{dr}^e , Ψ_{qr}^e , Ψ_{dm}^e and Ψ_{qm}^e the voltage, current and flux in d- and q-axis of stator, rotor (referred to stator

side) and air gap, respectively. In (5) and (6) the transient parts are not taken into account, because the iron losses are significant in high frequency area, in which the induced voltage by rotation is much larger than by self-induction.

Furthermore, the flux linkage equations are defined:

$$\Psi_{ds}^e = L_s i_{ds}^e + L_m i_{dr}^e - L_m i_{dfe}^e \quad (7)$$

$$\Psi_{dr}^e = L_r' i_{dr}^e + L_m i_{ds}^e - L_m i_{dfe}^e \quad (8)$$

$$\Psi_{dm}^e = L_m i_{ds}^e + L_m i_{dr}^e - L_m i_{dfe}^e \quad (9)$$

$$\Psi_{qs}^e = L_s i_{qs}^e + L_m i_{qr}^e - L_m i_{qfe}^e \quad (10)$$

$$\Psi_{qr}^e = L_r' i_{qr}^e + L_m i_{qs}^e - L_m i_{qfe}^e \quad (11)$$

$$\Psi_{qm}^e = L_m i_{qs}^e + L_m i_{qr}^e - L_m i_{qfe}^e \quad (12)$$

Where L_s , L_r' and L_m are the stator, rotor (referred to stator side) and the mutual inductances.

The calculation of the entire losses of the IM is based on these equations. To simplify the computation the rotor flux frame is applied with the electric angular frequency:

$$\omega_e = \frac{R_r' i_{qs}^e}{L_r' i_{\mu}^e} + \omega_r \quad (13)$$

Where i_{μ}^e represents the magnetic current. In rotor flux frame we obtain the following equations from (5), (6), (9) and (12):

$$i_{dfe}^e = \frac{\frac{\sigma_2}{1+\sigma_2} (\omega_e L_m)^2}{R_m^2 + \frac{\sigma_2}{1+\sigma_2} (\omega_e L_m)^2} i_{ds}^e - \frac{\frac{\sigma_2}{1+\sigma_2} \omega_e L_m R_m}{R_m^2 + \frac{\sigma_2}{1+\sigma_2} (\omega_e L_m)^2} i_{qs}^e \quad (14)$$

$$i_{qfe}^e = \frac{\omega_e L_m R_m}{R_m^2 + \frac{\sigma_2}{1+\sigma_2} (\omega_e L_m)^2} i_{ds}^e + \frac{\frac{\sigma_2}{1+\sigma_2} (\omega_e L_m)^2}{R_m^2 + \frac{\sigma_2}{1+\sigma_2} (\omega_e L_m)^2} i_{qs}^e \quad (15)$$

Where σ_2 denotes the rotor leakage coefficient. The description of the entire losses of the IM can be then derived as (16), which is dependent on stator d- and q-currents and electric angular frequency of rotor flux.

$$P_{\text{loss}} = \left\{ R_s + \frac{1}{\left[R_m^2 + \frac{\sigma_2}{1+\sigma_2} (\omega_e L_m)^2 \right]^2} \left[\left(\frac{\sigma_2}{1+\sigma_2} \right)^2 (\omega_e L_m)^4 R_m + (\omega_e L_m)^2 R_m^3 + \left(\frac{1}{1+\sigma_2} \right)^2 (\omega_e L_m)^2 R_m^2 R_r' \right] \right\} \cdot i_{ds}^e{}^2 + \frac{1}{\left[R_m^2 + \frac{\sigma_2}{1+\sigma_2} (\omega_e L_m)^2 \right]^2} \left(\frac{1}{1+\sigma_2} \right)^2 \omega_e L_m R_m^2 \left[\sigma_2 (\omega_e L_m)^2 - R_m R_r' \right] \cdot i_{ds}^e \cdot i_{qs}^e + \left\{ R_s + \frac{1}{\left[R_m^2 + \frac{\sigma_2}{1+\sigma_2} (\omega_e L_m)^2 \right]^2} \left[\left(\frac{\sigma_2}{1+\sigma_2} \right)^2 (\omega_e L_m)^4 R_m + \left(\frac{\sigma_2}{1+\sigma_2} \right)^2 (\omega_e L_m)^2 R_m^3 + \left(\frac{1}{1+\sigma_2} \right)^2 R_m^4 R_r' \right] \right\} \cdot i_{qs}^e{}^2 \quad (16)$$

3. Proposed Optimum Control Scheme

By using the machine loss description derived in the last section and the system constraint formulations the new optimum control scheme will be introduced in the following.

3.1 System Constraints

The system constraints of IM are represented by stator current and voltage limits, which are given as:

$$i_{ds}^e{}^2 + i_{qs}^e{}^2 \leq I_{dqmax}^2 \quad (17)$$

$$u_{ds}^e{}^2 + u_{qs}^e{}^2 \leq U_{dqmax}^2 \quad (18)$$

It is obvious that the current limit is described as a circle with constant radius and centered at origin in $i_{ds}^e - i_{qs}^e$ axis, whereas the case of the voltage limit is much more complicated. Substituting (7), (10), (14) and (15) into (1) and (2) we obtain:

$$u_{ds}^e = k_1(\omega_e)i_{qs}^e - k_2(\omega_e)i_{qs}^e + k_3(\omega_e)i_{ds}^e \quad (19)$$

$$u_{qs}^e = l_1(\omega_e)i_{ds}^e - l_2(\omega_e)i_{ds}^e + l_3(\omega_e)i_{qs}^e \quad (20)$$

Where k_1 , k_2 , k_3 , l_1 , l_2 and l_3 are frequency-varying coefficients, which increase monotonically with ω_e . By applying the machine parameters into both equations we get the coefficient values by $\omega_e = \omega_N$ and $\omega_e = 4\omega_N$.

As shown in Tab. 1 the coefficients k_2 and l_1 dominate the voltage values over the frequency domain. Therefore, (19) and (20) can be approximated by

$$u_{ds}^e = -\omega_e \sigma L_s i_{qs}^e \quad (21)$$

$$u_{qs}^e = \omega_e L_s i_{ds}^e \quad (22)$$

Where σ denotes the total leakage coefficient. Thus, the voltage limit can be represented by an ellipse at origin, which shrinks by increasing the frequency.

Table 1. Frequency-varying coefficients

Coeffs.	$\omega_e = \omega_N$	$\omega_e = 4\omega_N$
k_1	1.37×10^{-3}	0.022
k_2	1.992	7.970
k_3	0.043	0.692
l_1	26.420	105.683
l_2	2.437×10^{-3}	0.155
l_3	0.043	0.692

3.2 Dynamical Torque Adaptation

Using MTPA the whole frequency domain can be divided into three regions, which is introduced in [2]. In the region under a certain frequency, generally the nominal frequency, only the current limit should be taken into account. Beyond the nominal frequency the voltage limit should be considered as well. There exists one frequency ω_c , over which the current limit is no more interesting, because the tangential point of torque and voltage curves is located inside the current-limit circle instead of on its edge. These both frequencies are determined by machine parameters and system constraints as following:

$$\omega_N = \frac{U_{dqmax}}{\sqrt{L_s^2 i_{dsN}^e{}^2 + \sigma^2 L_s^2 (I_{dqmax}^2 - i_{dsN}^e{}^2)}} \quad (23)$$

$$\omega_N = \sqrt{\frac{L_s^2 + \sigma^2 L_s^2}{2\sigma^2 L_s^4}} \frac{U_{dqmax}}{I_{dqmax}} \quad (24)$$

The current values of applied torque by MPTA are located at the tangential point of loss and torque curves:

$$P_{loss} = A(\omega_e)i_{ds}^e{}^2 + B(\omega_e)i_{ds}^e i_{qs}^e + C(\omega_e)i_{qs}^e{}^2 \quad (25)$$

$$i_{qs}^e = \frac{T_e}{D i_{ds}^e} \quad (26)$$

Substituting (26) in (25) and with $\frac{\partial P_{loss}}{\partial i_{ds}^e} = 0$ we obtain

$$\frac{i_{qsopt}^e}{i_{dsopt}^e} = \sqrt{\frac{A(\omega_e)}{C(\omega_e)}} = \text{const.} \quad (27)$$

for a certain ω_e . By substituting (24) in (27) the gradient at point ω_c is equal to $1/\sigma$. Fig. 2 illustrates the trajectory of operating points according to MTPA.

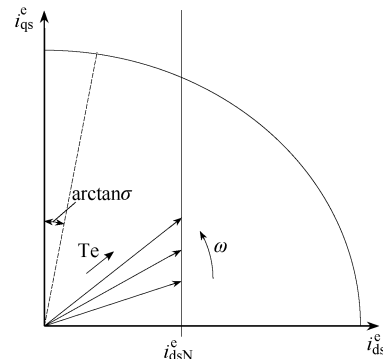


Fig. 2. Trajectory of MTPA

By means of MTPA the losses of an IM can be reduced significantly. However, in the transient procedures, in which the system constraints are activated, the loss

minimization curve can not be guaranteed anymore. In the following the approach with dynamical torque adaptation will be introduced.

In Fig. 3 the whole frequency domain is divided into three cases by two frequencies given in (23) and (24). The blue dashed lines 0A and 0C illustrate the possible trajectories describing tangential points of loss minimization and torque curves by a certain rotor flux speed. The red lines represent the constraint/boundary lines to be considered. In each case the whole region can be divided into several sub regions as shown in figures.

Fig. 3(a) describes the basic speed area, in which only current limit should be considered. The whole region is divided by the boundary lines and the line 0E between origin and nominal point. If the gradient of the tangential point trajectory by frequency ω is smaller than 0E, e.g. 0A, only sub regions 1 and 2 have to be observed. The optimum current point follows 0A as long as the required torque is

smaller than the one attained at point A. In case of a torque requirement larger than this value in the transient procedure, e.g. T_e in the figure, the MTPA takes the intersection of current and voltage limit lines (point E), whereat the proposed scheme calculates the minimal loss and chooses the admissible current combination at point B, which provides the adapted torque. In case that the optimum current trajectory lies over 0E, e.g. 0C, the point D is chosen.

Fig. 3(b) illustrates the field-weakening area, in which both current and voltage limits have to be taken into account. Point E denotes the intersection of current and voltage limit lines. Different to the basic speed area, the gradient of 0E is speed-varying and should be calculated for current frequency. In case of 0A the chosen point B must not be on the line of nominal magnetic current, but it is also possible, that point B lies on the voltage limit curve.

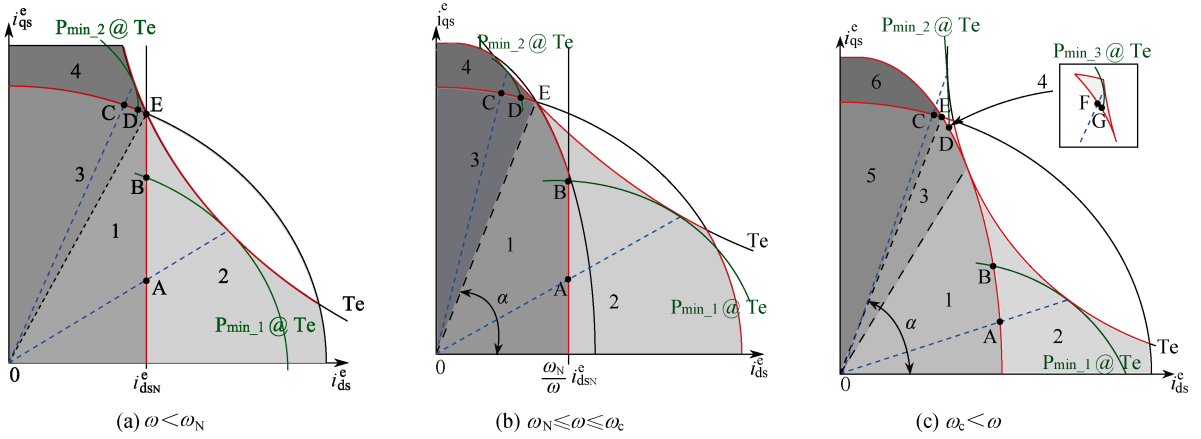


Fig. 3. Dynamical torque adaptation and current determination.

In the high speed area, in which only voltage limit has to be considered, the gradient of 0E in Fig. 3(c) is speed-varying and should be updated according to the speed as in Fig. 3(b). In case of 0C the point D is determined by the intersection of loss minimization curve, which is tangent to the torque curve, and the voltage limit curve. In sub region 4 instead of point F point G is applied.

The adaptation information is then returned to the speed controller to obviate windup effect. Depending on the location of the operating point, different control strategies should be approached, which are introduced in the following. For the complete calculation the following functions are utilized:

- $f_1(i_{ds}^e, i_{qs}^e) = i_{ds}^e{}^2 + i_{qs}^e{}^2 - i_{dqmax}^2$
- $f_2(i_{ds}^e, i_{qs}^e) = (\omega_e L_s i_{ds}^e)^2 + (\omega_e \sigma L_s i_{qs}^e)^2 - U_{dqmax}^2$
- $f_3(i_{ds}^e, i_{qs}^e, P) = A(\omega_e) i_{ds}^e{}^2 + B(\omega_e) i_{ds}^e i_{qs}^e + C(\omega_e) i_{qs}^e{}^2 - P$

- $f_4(i_{ds}^e, i_{qs}^e) = D i_{ds}^e i_{qs}^e$

According to the location of operating point one of the following strategies will be executed:

- 1) $i_{dsopt}^e = i_{dsmin}^e$; $i_{qsopt}^e = i_{qsmin}^e$; $T_{eopt}^* = T_e^*$.

- 2) $i_{dsopt}^e = i_{dsN}^e$;

$$\text{solve } f_3(i_{dsmin}^e, i_{qsmin}^e) = 0 \text{ and get } P_{min};$$

$$\text{solve } f_3(i_{dsN}^e, P_{min}) = 0 \text{ and get } i_{qsopt}^e;$$

$$T_{eopt}^* = f_4(i_{dsopt}^e, i_{qsopt}^e).$$

- 3) solve $f_3(i_{dsmin}^e, i_{qsmin}^e) = 0$ and get P_{min} ;

$$\text{solve } f_1 = 0 \text{ and } f_3(P_{min}) = 0 \text{ and get } i_{dsopt}^e \text{ and } i_{qsopt}^e;$$

$$T_{eopt}^* = f_4(i_{dsopt}^e, i_{qsopt}^e).$$

- 4) solve $f_3(i_{dsmin}^e, i_{qsmin}^e) = 0$ and get P_{min} ;

solve $f_2=0$ and $f_3(P_{\min})=0$ and get $i_{ds\text{opt}}^e$ and $i_{qs\text{opt}}^e$;
 $T_{\text{eopt}}^* = f_4(i_{ds\text{opt}}^e, i_{qs\text{opt}}^e)$.

Fig. 4 gives an overview of the strategy determination for the proposed control scheme.

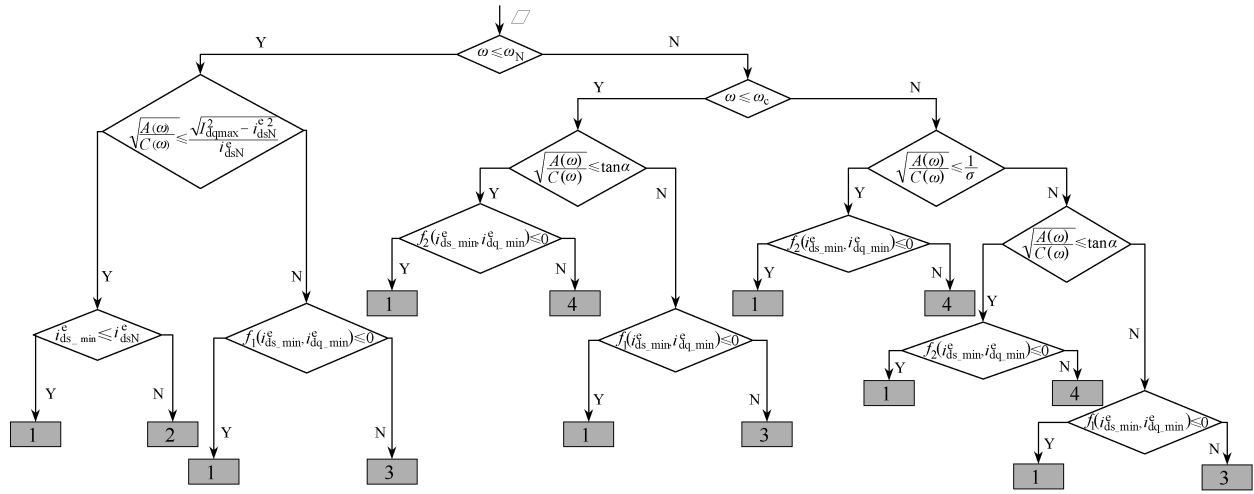


Fig.4. Flow diagram of the proposed control scheme.

3.3 Optimum Current Control

To assure drive dynamic and simultaneously to suppress overshooting of flux-generating current, an optimum current control using generalized predictive control (GPC) is introduced for the proposed control scheme. GPC developed by Clarke et al [13]. is one of the most popular model predictive control (MPC) methods in industry and academia and can deal with single-input-single-output (SISO) plants.

Every MPC method consists of three fundamental components:

- Prediction model
- Cost function
- Control law

The GPC uses Controlled Auto-regressive Integrated Moving Average (CARIMA) (see [14] for more information) to describe the plant, which is given by

$$A(z^{-1})y(t) = B(z^{-1})z^{-d}u(t-1) + C(z^{-1})\frac{e(t)}{\Delta} \quad (28)$$

with

$$\Delta = 1 - z^{-1}$$

Where A and B depict the system behavior, $e(t)$ the noise, d the dead time of the system and C polynomial can be designed for an internal filter. Using this prediction model the system output can be predicted, which is based on the future control set and past outputs and controls. Therefore, the predicted outputs in finite prediction horizon y can be described as

$$y = Gu + f \quad (29)$$

Where u is the sequence of control actions in the future, G is the derived matrix. This term depends on the control actions in future and is called forced response. f is the information about the past, which is free from the control actions and therefore is named free response.

The cost function of MPC determines the behavior of the controlled system. It can be defined differently for various aims. The general expression is given by:

$$\mathcal{J}(N_1, N_2, N_u) = \sum_{j=N_1}^{N_2} \mu_j (w_{t+j} - \hat{y}_{t+j})^2 + \sum_{j=1}^{N_u} \lambda_j A_u(t+j-1)^2 \quad (30)$$

N_1 and N_2 are the start and the end step of the prediction horizon. In case of the existence of dead time in system, N_1 should be defined in such a way, that the dead time is taken into account. N_u denotes the control horizon, which gives the control action steps. Beyond the control horizon, the control signal should not be changed anymore. The first term of the cost function describes the ability to track the reference signal. The bigger the weighting factor μ_j is, the faster the reference can be tracked. The second term of the cost function specifies the actuating energy used within the prediction horizon. For purpose of simplification of parameter tuning, the weighting factor μ can be set to 1 and only λ has to be modified.

Substituting (29) into (30) we obtain the cost function represented by the control actions in the future:

$$\mathcal{J} = (Gu + f - w)^T (Gu + f - w) + \lambda u^T u \quad (31)$$

Where w is the sequence of the reference values in the prediction horizon. By partial derivative of J with respect to u and making this gradient equal to zero, the control law can be attained. The control action in the next time step is calculated by adding the first element of u to the control signal in the last time step. Only this value is applied to the system and the complete optimization procedure will be repeated again based on the updated information in the next time step. Therefore, MPC is also called Receding Horizon Control (RHC).

Fig. 5 gives the structure of the system, which is controlled by GPC. According to the prediction model, the past system outputs and the control actions both in the past and future, the predictor provides the system outputs a priori. The optimizer decides the control law by minimizing the cost function. The control action in the next time step is then applied as input to the system.

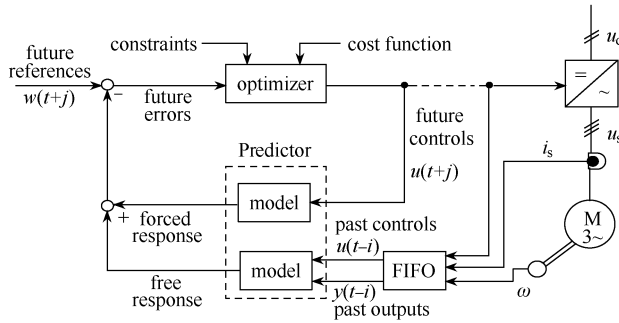


Fig. 5. Structure of Generalized Predictive Control [15]

In Fig. 6 an overview of the control structure is depicted. Because the speed controller using GPC can achieve a high dynamic of the speed control loop through the optimization procedure, the flux control in inner loop can be dispensed without deterioration of the system dynamic. In the next section the simulation results of conventional $1/\omega_r$, steady state MTPA and the proposed scheme will be compared.

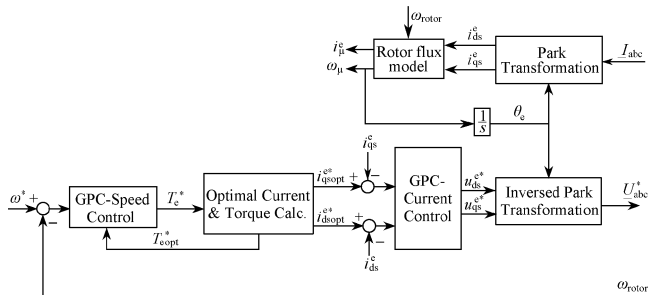


Fig. 6. Block Diagram Optimum Current Control

4. Simulation Results

The complete simulation process is defined as follows:

Table 2. Simulation process

Period(s)	Reference Speed(r/min)	Load Torque(N · m)
A: 0-2	1000	5
B: 2-3.5	2000	50
C: 3.5-5	4500	30
D: 5-8	1000	10
E: 8-10	1000	20

Firstly the trajectories of the stator current will be analyzed. Fig. 7 illustrates the trajectories in transient procedure from period D to E of conventional $1/\omega_r$, steady state MTPA and the proposed scheme, which are marked by the solid lines in blue, red and green, respectively. In the steady states of D and E the IM works at different operating points, which are distinguished by soft and solid dots. Because the latter two schemes are based on the same principle in steady states, the operating points lie upon each other. The two dashed lines depict the load torques of D and E. As the reference speeds in both periods are the same and the impact of load torque change on the speed is limited, the gradient of the optimal stator current trajectories of MTPA and the proposed scheme can be considered as constant. It is easy to identify in the figure, the conventional $1/\omega_r$ keeps the rotor flux constant in the basic speed area. Thus, the trajectory lies in parallel to the i_{qs} -axis. The green solid line corresponds with the optimal trajectory with the gradient in (27), whereas by MTPA the stator current deviates from the optimal trajectory due to the overshooting of d-axis current.

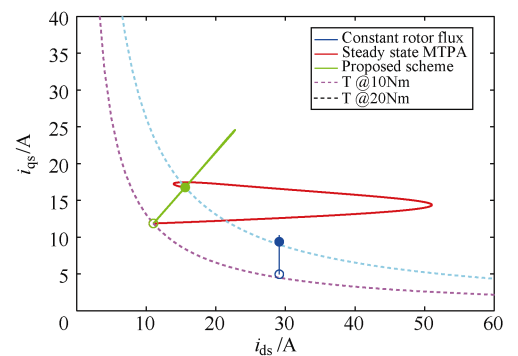


Fig. 7. Stator current trajectory

In the following the transient procedures with activated system limits will be discussed. Fig. 8 shows the machine loss development of three control schemes during the transient procedures from B to C and C to D as well as the steady state in C, in which the IM works in the field-weakening area. It is evident that during the transient procedures the IM power losses are reduced significantly

by using the proposed scheme when compared to steady state MTPA. In the steady state with low load (after 5.4 seconds), both the proposed scheme and MTPA show a better efficiency than the conventional $1/\omega_r$ control.

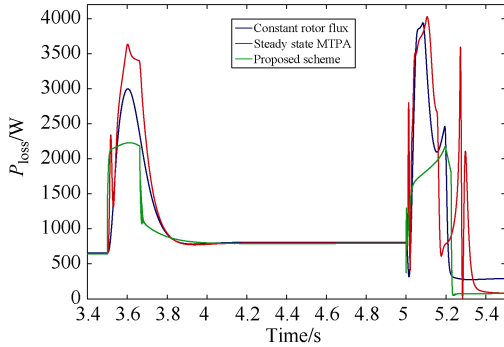


Fig. 8. Power loss in transient states with system limits

Fig. 9 gives the energy losses of the IM during the complete drive cycle. The control parameters of these three schemes are chosen in such a way, that the system dynamics are similar. The gradients of the energy loss curve, which describes the power loss, of the conventional control scheme in steady states are generally larger than those of the other schemes. Furthermore, in the transient procedures the increase of energy loss curve by the proposed scheme is in principle slower than the one by MTPA. The results show the energy efficiency of the conventional $1/\omega_r$ method is about 88.42%, 89.89% by MTPA and 91.81% by the proposed control scheme.

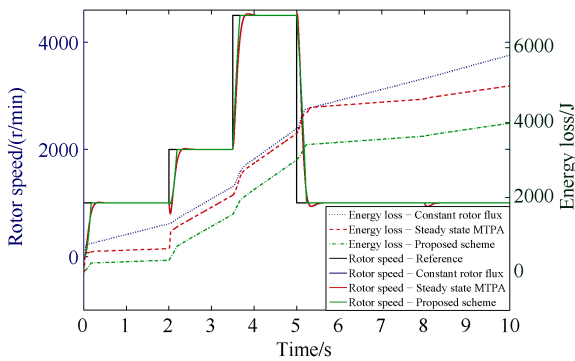


Fig. 9. Energy loss development during the drive cycle.

5. Conclusions

In this paper the model of an IM including iron losses is proposed, in which the iron losses are represented by a resistance connected in parallel to the mutual inductance. The iron losses are formulated by using iron loss current instead of the air gap voltage, which is more accurate. Based on this power loss description, an optimum current

control scheme considering system limits is studied. The simulation results confirm that by means of the proposed scheme the power loss can be reduced significantly in case of transient states and system limit activation.

References

- [1] A. Kusko, and D. Galler, "Control means for minimization of losses in ac and dc motor drives." *Industry Applications, IEEE Transactions on*, Vol. 19, No. 4, pp. 561-570, 1983.
- [2] S. Kim, and S. Sul, "Maximum Torque Control of an Induction Machine in the Field Weakening Region," *Industry Applications, IEEE Transactions on*, Vol.31, No.4, pp. 787-794, Jul. 1995.
- [3] J. F. Stumper, A. Döttinger, and R. Kennel, "Loss Minimization of Induction Machines in Dynamic Operation," *Energy Conversion, IEEE Transactions on*, Vol. 28, No. 3, pp. 726-735, Sep. 2013.
- [4] R. D. Lorenz, and S. M. Yang, "Efficiency-optimized flux trajectories for closed-cycle operation of field-orientation induction machine drives," *Industry Applications, IEEE Transactions on*, Vol. 28, No. 3, pp. 574-580, 1992.
- [5] G. O. Garcia, J. C. M. Luis, R. M. Stephan, and E. H. Watanabe, "An efficient controller for an adjustable speed induction motor drive," *Industrial Electronics, IEEE Transactions on*, Vol. 41, No. 5, pp. 533-539, 1994.
- [6] F. Fernandez-Bernal, A. Carcia-Cerrada, and R. Faure, "Model-based loss minimization for dc and ac vector-controlled motors including core saturation," *Industry Applications, IEEE Transactions on*, Vol. 36, Issue: 3, pp. 755-763, 2000.
- [7] S. Lim, and K. Nam, "Loss-minimising control scheme for induction motors," *IEE Proceedings on Electric Power Applications*, Vol. 151, pp. 385-389, Jul. 2004.
- [8] G. Gallegos-López, F. S. Gunawan, and J. Walters, "Current Control of Induction Machines in the Field-Weakened region," *Industry Applications, IEEE Transactions on*, Vol. 43, No. 4, pp. 981-989, 2007.
- [9] D. S. Kirschen, D. W. Novotny, and T. A. Lipo, "On-line efficiency optimization of a variable frequency induction motor drive," *Industry Applications, IEEE Transactions on*, Vol. 21, No.4, pp. 610-616, 1985.
- [10] S. K. Sul, and M. H. Park, "A novel technique for optimal efficiency control of a current-source inverter-fed induction motor," *Power Electronics, IEEE Transactions on*, Vol. 3, Issue:2, pp. 192-199, 1988.
- [11] G. K. Kim, I. J. Ha, and M. S. Ko, "Control of induction motors for both high dynamic performance and high power efficiency," *Industrial Electronics, IEEE Transactions on*, Vol. 39, No. 4, pp. 323-333, 1992.
- [12] D. W. Novotny, and T. A. Lipo, "Vector Control and Dynamics of AC Drives". Oxford Science, 1996.
- [13] D. W. Clarke, C. Mohtadi, and P. S. Tuffs, "Generalized Predictive Control. Part I. The Basic Algorithm," *Automatica*, Vol. 23, No. 2, pp. 137-148, 1987.
- [14] J. A. Rossiter, "Model-based Predictive Control-A Practical Approach". CRC Press, 2005.
- [15] A. Linder, R. Kanchan, R. Kennel, and P. Stolze, "Model-Based Predictive Control of Electric Drive". Cuvillier Verlag Göttingen, 2010.



Zheng Hu received his diploma in Computer Science in 2008 and diploma in Industrial Engineering in 2011 at the RWTH Aachen University, Germany. Until January 2012, he worked as Software Engineer at Gesellschaft für Industrieforschung mbH in Alsdorf, Germany in the field of automatic transmission controls. Currently, he is a Research Associate at the Institute of Electrical Machines of RWTH Aachen University and focuses his work on optimal control of electric drive systems.



Qian Liu finished his Bachelor in Electrical Engineering in 2008 at Shanghai Jiao Tong University, China. In 2011 he received his Master degree in Control Engineering from Technical University of Kaiserslautern, Germany. Currently he is a research associate in the Institute of Electrical Machines at RWTH Aachen University, Germany. His research focuses on wind turbines, motor drive system and power electronics.



Kay Hameyer (M'96-SM'99) received his M.Sc. degree in electrical engineering from the University of Hannover and his Ph.D. degree from the Berlin University of Technology, Germany. After his university studies he worked with the Robert Bosch GmbH in Stuttgart, Germany as a Design Engineer for permanent magnet servo motors and vehicle board net components. Until 2004 Dr. Hameyer was a full Professor for Numerical Field Computations and Electrical Machines with the KU Leuven in Belgium. Since 2004, he is full professor and the director of the Institute of Electrical Machines (IEM) at RWTH Aachen University in Germany. 2006 he was vice dean of the faculty and from 2007 to 2009 he was the dean of the faculty of Electrical Engineering and Information Technology of RWTH Aachen University. His research interests are numerical field computation and optimization, the design and controls of electrical machines, in particular permanent magnet excited machines, induction machines and the design employing the methodology of virtual reality. Since several years Dr. Hameyer's work is concerned with the development of magnetic levitation for drive systems, magnetically excited audible noise in electrical machines and the characterization of ferro-magnetic materials. Dr. Hameyer is author of more than 250 journal publications, more than 500 international conference publications and author of 4 books. Dr. Hameyer is a member of VDE, IEEE senior member, fellow of the IET.